ROYAL SOCIETY
OF CHEMISTRY

PAPER

Check for updates

Effects of selenium incorporation on the performance of polythiophene based organic electrochemical transistors†

Meisi Li,‡[a] Wang Feng,‡[a] Yu Lan,[a] Yimin Sun,[a] Ping Li,*[b] Jianfeng Li,[c] Wanli Yang,[c] Hongxiang Li,[d] Junqiao Ding ⓘ[a] and Jianhua Chen ⓘ*[a]

Selenium incorporation is a widely used strategy for achieving high mobility semiconductors for a variety of organic optoelectronic devices, but it has received less attention in organic electrochemical transistors (OECTs). Herein, we developed two polythiophene derivatives (Pg2T-S and Pg2T-SVS) containing different selenophene loadings, as well as a selenophene-free polythiophene (Pg2T-T) as the control. The effects of selenium substitution/incorporation on the optical, electrical, electrochemical, and OECT performance of polythiophene-based organic mixed ionic–electronic conductors are systematically investigated. We discovered that introduction of selenium increases quinoidal character and crystallinity, which is beneficial for charge transport but makes ion penetration more challenging. In contrast, increasing selenium content increases the dipole moment and ion–polymer interaction, which is helpful for ion doping and volumetric capacitance but detrimental to charge transport. Therefore, appropriate selenium content should be evaluated to balance the trade-off between charge transfer and volumetric capacitance. As a result, Pg2T-S with moderate selenium loading achieves a high μC^* of 332.7 F cm^{-1} V^{-1} s^{-1} with increased μ of 1.31 cm^2 V^{-1} s^{-1} and maintains the C^* value of 254 F cm^{-3}. It also has a quick τ_{on}/τ_{off} of 10.76 ms/5.90 ms and outstanding operational stability. Further introducing selenium boosts the dipole moment and ion–polymer interaction and therefore increased C^*, but suppressed μ, resulting in inefficient μC^*. We indicated that systematic balancing of the effects of selenium incorporation is necessary for the development of mixed ionic–electronic conductors for high-performance OECTs.

Introduction

Organic electrochemical transistors (OECTs) have emerged as attractive bioelectronic devices for application in bio-interfaced electronics, chemical sensing, digital logic, and neuromorphic computing owing to their high transconductance, biocompatibility, and sensitivity to biological signals.[1–6] The operation of OECTs depends extensively on their active channel materials,

[a] *School of Chemical Science and Technology, Yunnan University, Kunming 650500, China*

[b] *State Key Laboratory for Mechanical Behavior of Materials, Center for Spintronics and Quantum System, School of Materials Science and Engineering, Xi'an Jiaotong University, Xi'an, Shaanxi 710049, People's Republic of China. E-mail: chenjianhua@ynu.edu.cn*

[c] *Department of Materials Science and Engineering, Southern University of Science and Technology (SUSTech), Shenzhen, Guangdong 518055, China. E-mail: pli@xjtu.edu.cn*

[d] *College of Polymer Science and Engineering, State Key Laboratory of Polymer Materials Engineering, Sichuan University, Chengdu 610065, China*

‡ These authors made equal contribution.

which are typically constructed of organic mixed ionic–electronic conductors (OMIECs).[7–9] OMIECs can be classified as p-type (hole transporting) and n-type (electron transporting) based on the carriers they transport, and they can operate in depletion mode (intrinsically doped) or accumulation mode (intrinsically undoped) depending on the doping level of their pristine state.[10] Up to now, the most widely used OMIEC in OECTs is a strongly doped mixture of poly(3,4-ethylenedioxy-thiophene): polystyrene sulfonate (PEDOT:PSS), which worked in depletion mode and had a substantially larger channel current than other OECTs in accumulation mode. Although PEDOT:PSS has demonstrated advantages in electrochemical stability, high conductivity, and commercial availability, the nature of its acidity and depletion working modes make further application for bio-interfaced electronics difficult due to unfavorable device stability and higher power consumption concerns.[11–13] Therefore, significantly greater effort has been dedicated to developing intrinsically undoped OMIECs.[14]

In order to evaluate the performance of OMIECs, the product of the electronic mobility and volumetric charge storage capacity (μC^*) is introduced as a figure of merit, according to
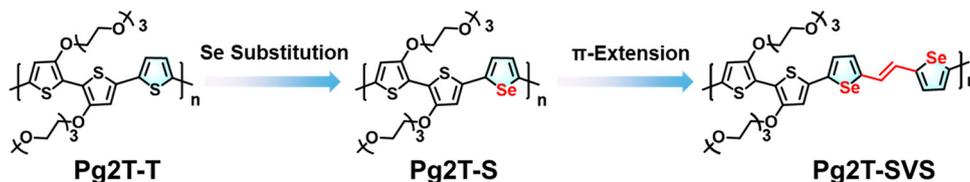
Chart 1 Molecular design strategy by selenium substitution and further π-extension for polythiophene-based organic mixed ionic–electronic conductors.

the equation below:

$$g_{m} = \frac{Wd}{L}\mu C^{*}(V_{Th} - V_{GS})$$

where g_{m} is the transconductance; W, L, and d represent the channel width, length, and film thickness, respectively; V_{Th} and V_{GS} are the threshold voltage and applied gate voltage, respectively. Apparently, μC^{*} is a nominally geometry- and bias-independent term and can be used to benchmark and compare material performance.[15]

Recently, a variety of hydrophilic ethylene glycol (EG) side chain modified polythiophenes have been reported and optimized due to their good backbone planarity, excellent charge transport properties, well maintained high capacity, and thereby promising μC^{*}. In 2016, Christian et al. developed the first polythiophene based OMIECs named P(g2T-T), which demonstrated a high μC^{*} of 167 ± 65 F cm^{-1} V^{-1} s^{-1} and outperformed PEDOT:PSS.[15,16] Thereafter, Alexander et al. developed a bithiophenthieno-based polythiophene named poly-(2-(3,3′-bis(2-(2-(2-methoxyethoxy)ethoxy)ethoxy)-[2,2′-bithiophen]-5-yl)thieno[3,2-b]thiophene), p(g2T-TT), exhibiting a significantly improved μC^{*} of 261 ± 29 F cm^{-1} V^{-1} s^{-1} originated from significantly enhanced electronic mobility (μ_{OECT}) of 0.95 cm^2 V^{-1} s^{-1} when compared to P(g2T-T).[17] In addition, manipulation of EG side chains including their length, distribution, regiochemical attachment, hydrophilicity, and so on, was realized to be an efficient strategy to increase OECT performance and stability.[13,18,19] The well-designed p(g2T2–g4T2)[15] and pgBTTT[10] attained exceptionally high μC^{*} of 522

and 502 ± 18 F cm^{-1} V^{-1} s^{-1}, respectively. These are among the highest for polythiophene-based OMIECs. The improvement was attributed to the much-improved mobility, fine-tuned water uptake, and balanced μ and C^{*}.

Apart from the strategies listed above, selenium (Se) substitution is an important strategy for achieving high mobility in organic semiconductors and has been extensively investigated in organic solar cells, organic field effect transistors, organic thermoelectric materials and so on. Compared to thiophene derivatives, selenophene analogs demonstrate increased polarizability, stronger intermolecular interaction, and superior aromaticity, attributable to the more extended lone pair electrons and larger van der Waals atomic radius of the Se atom instead of sulfur.[20–23] Guo et al. have recently employed a Se substitution strategy to develop high performance n-type OMIECs with enhanced charge-transport properties and increased ion-uptake capabilities. The newly reported f-BSeI2g-SVSCN achieved a record μC^{*} of 191.2 F cm^{-1} V^{-1} s^{-1} with a remarkable C^{*} value of 387.2 F cm^{-3} and $\mu_{e,OECT}$ of 0.48 cm^2 V^{-1} s^{-1} for n-type OECTs.[24] However, the mechanisms underlying this performance gain are unclear, and Se substitution for p-type OMIECs is rarely used.

With these considerations in mind, we designed and synthesized two selenophene-incorporated polythiophenes (Pg2T-S and Pg2T-SVS, Chart 1), as well as a control selenophene-free polythiophene (Pg2T-T), to investigate the effects of Se incorporation on the p-type OECT performance of polythiophene based OMIECs. It should be noticed that Rivnay et al. conducted similar studies on heteroatom substitution (furan, thiophene, selenophene, and tellurophene) in conjugated polymers.[25] They found that the polymer microstructure plays an important role in mixed conduction, with a Te-containing polymer achieving the highest μ_{hole} value of 3.60 cm^2 V^{-1} s^{-1} and μC^{*} of 483 F cm^{-1} V^{-1} s^{-1} due to well-oriented edge-on 3D crystallite orientation. In addition, a Se-containing polymer exhibited an unfavorable μC^{*} of only 91 F cm^{-1} V^{-1} s^{-1}, which is even lower than that of thiophene-based polymers (288 F cm^{-1} V^{-1} s^{-1}). In this work, we comprehensively evaluated the influence of selenophene incorporation on the dipole moment, crystallinity, redox capability, and chloride ion (Cl^{-}) interaction of polymers, and their OECT performance including μ, C^{*}, μC^{*}, transient response, and stability. Furthermore, the structure–property performance relationship has been preliminarily established. We found that increasing selenophene loading improves crystallinity and intermolecular interaction, which is beneficial for charge transport while

Jianhua Chen obtained his PhD from Xiangtan University in 2016, under the supervision of Prof. Weiguo Zhu. From 2016 to 2018, he worked as a postdoctoral scholar in the lab of Prof. Xugang Guo at the Southern University of Science and Technology. He then completed his postdoctoral training with Tobin J. Marks and Antonio Facchetti at Northwestern University before joining Yunnan University as an associate professor in 2021. His research focuses on polymer semiconductors and devices.

Jianhua Chen

7936 | *J. Mater. Chem. C*, 2024, **12**, 7935–7942

This journal is © The Royal Society of Chemistry 2024

preventing ion penetration. In contrast, the dipole moment and chloride ion (Cl⁻)–polymer cation (P⁺) interaction increase as the selenophene loading increases, revealing efficient doping and high C^* values. Consequently, Pg2T-S with moderate selenophene loading exhibits the highest μC^* of 332.7 F cm⁻¹ V⁻¹ s⁻¹, with a more balanced μ of 1.31 cm² V⁻¹ s⁻¹ and C^* of 254 F cm⁻³, compared to Pg2T-T (288.9 F cm⁻¹ V⁻¹ s⁻¹) and Pg2T-SVS (285.0 F cm⁻¹ V⁻¹ s⁻¹). Our findings suggest that selenium substitution has a complicated influence on material properties rather than charge transport mobility, particularly for OECTs with mixed ionic–electronic conduction.

Results and discussion

Prior to polymer synthesis, density functional theory (DFT) calculations were carried out to investigate the influence of selenium incorporation on optimal geometries, electronic structures, and dipole moments. As shown in Fig. 1, all polymers have good backbone planarity, with dihedral angles between adjacent aromatic rings less than 2 degrees. As selenophene loading and π-extension increase, the dipole moments increase from 1.12 Debye for Pg2T-T to 1.15 and 1.99 Debye for Pg2T-S and Pg2T-SVS, respectively, which is partially due to the higher polarizability of selenium than sulfur atoms.[20] The frontier molecular orbitals of polymers are illustrated in Fig. S1 (ESI†), and both highest occupied molecular orbital (HOMO) and lowest unoccupied molecular orbital (LUMO) wavefunctions are delocalized across the entire polymer backbone. Such good backbone planarity and efficient electron delocalization characteristics may be responsible for high hole mobility. The calculated HOMO and LUMO energy levels are −4.08/−2.01 eV, −4.08/−2.06 eV, and −4.15/−2.35 eV for Pg2T-T, Pg2T-S, and Pg2T-SVS, respectively. Apparently, selenium incorporation efficiently lowers the polymer's LUMO energy levels and thus optical bandgaps.

The synthetic route to the three polymers is shown in Scheme S1 (ESI†). And all polymers were synthesized according to classical Stille coupling polymerization, with details summarized in the ESI.† In general, selenium incorporation reduces solubility. Therefore, the polymer solubility is fine-tuned by controlling reaction concentration and times. The molecular weights were initially determined using gel-permeation chromatography (GPC) measurements using chloroform as the eluent. However, no visible signals were detected. Therefore, high-temperature GPC (150 °C) with 1,2,4-tricholorobenzene (TCB) as the eluent was carried out and a molecular weight (M_w) of 19.5 kDa for Pg2T-T, 13.3 kDa for Pg2T-S, and 21.5 kDa for Pg2T-SVS was recorded, with the corresponding polydispersities (PDI) of 2.35, 2.38 and 2.65, respectively. Note that Pg2T-T with reduced molecular weight exhibits greater crystallinity and structural ordering, as well as increased μ and μC^* compared to high molecular weight ones.[26] And the molecular weights of Pg2T-T, Pg2T-S and Pg2T-SVS are similar, allowing for reliable comparison. The thermal properties were investigated using thermogravimetric analysis (TGA, see Fig. S2, ESI†). All polymers show good thermal stability, with the T_d (5%-decomposition temperature) of over 213 °C under a N₂ atmosphere.

The UV-Vis-NIR absorption spectra of polymers in solution and thin films were recorded to investigate the influence of selenium incorporation on the optical properties of polythiophene-based polymers. In solution (Fig. 2a), Pg2T-S and Pg2T-SVS show significantly red-shifted absorption compared to Pg2T-T, owing to Se-based polymer's greater quinoidal character.[27] This behavior is accentuated in the thin film condition (Fig. 2b), where the maximum absorption peak is red-shifted to 635 nm for Pg2T-S and 650 nm for Pg2T-SVS, compared to 607 nm for Pg2T-T. In addition, Pg2T-SVS and Pg2T-S illustrate more pronounced 0–0 vibration than Pg2T-T due to strong aggregation and intermolecular interaction of selenium-incorporated polymers. It is worth noting that a weak broad absorption peak around 1000 nm is observed in the thin films, which should arise from the absorption of polarons. We suspect that the chlorine radical forms after light irradiation of residual chloroform in films and then slightly dopes the polymer films. Our hypothesis is confirmed by the UV-Vis-NIR
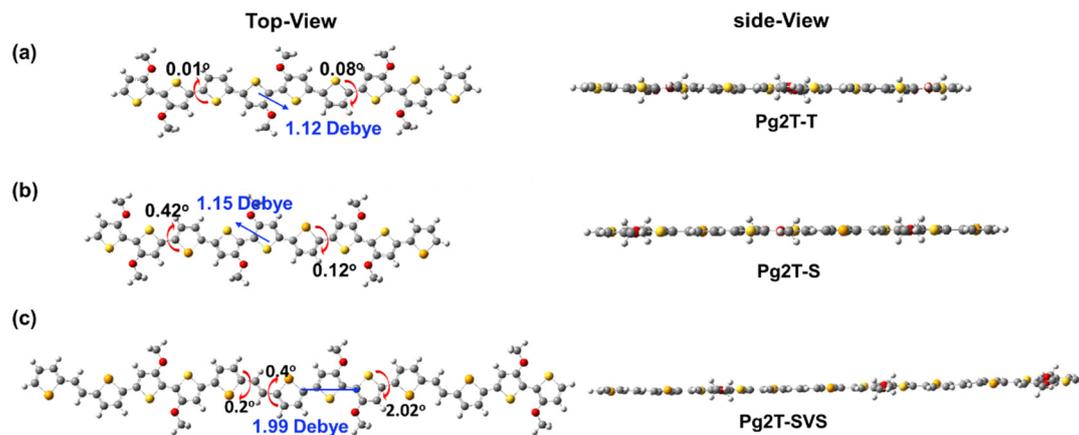

Fig. 1 Optimized geometries of the polymer with three repeating units of (a) Pg2T-T, (b) Pg2T-S, and (c) Pg2T-SVS. DFT calculations were performed at the B3LYP/6-311G(d,p) level. Branched glycol side chains were replaced with methyl groups to simplify the calculations.
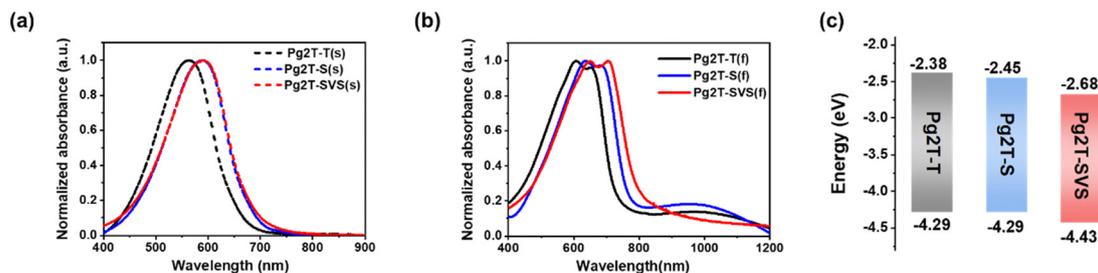
This journal is © The Royal Society of Chemistry 2024

J. Mater. Chem. C, 2024, **12**, 7935–7942 | **7937**

Fig. 2 The UV-vis absorption spectra of Pg2T-T, Pg2T-S, and Pg2T-SVS in (a) solution and (b) as in the thin film state. (c) Energy level diagram.

absorption spectra of polymers in chloroform under 365 nm irradiation for various time periods (Fig. S3, ESI†). As the illumination period increases, the neutral state absorption bands from 400 to 750 nm fade, while new bands from 800 to 1200 nm for doped states become more prominent.

The HOMO and LUMO energy levels were further evaluated by cyclic voltammetry (CV) measurements, as shown in Fig. S4a (ESI†) and Fig. 2c, with CV results summarized in Table 1. Compared to Pg2T-T (−4.29/−2.38 eV), Pg2T-S and Pg2T-SVS have lower HOMO/LUMO energy levels of −4.29/−2.45 and −4.43/−2.68 eV, respectively. Apparently, selenium introduction causes deeper molecular energy levels, particularly LUMO energy levels, which is consistent with prior findings.[20,22] The polymer stability in acetonitrile solution was further investigated as shown in Fig. S4 (ESI†). After 200 redox cycles, all polymers show negligible decrease of current, demonstrating remarkable electrochemical stability.

CV sweep measurements in 0.1 M NaCl electrolyte were further carried out (Fig. 3a–c). Both Pg2T-T and Pg2T-S show a first oxidation peak around 0.2 V, lower than Pg2T-SVS (0.3 V), consistent with the HOMO alignment mentioned earlier. In addition, all polymers exhibit good electrochemical stability in aqueous solution under bias in the range of −0.40 V to 0.65 V versus Ag/AgCl for 50 cycles, which is favorable for steady OECT operation.

Spectroelectrochemical measurements were utilized to investigate the electrochemical activity of polymers, as shown in Fig. 3d–f. All polymers have identical electrochromic activities. The absorption spectrum only minimally changed under bias from −0.4 V to 0.1 V, indicating weak doping. As the bias is increased from 0.1 V to 0.65 V, the neutral state absorption

bands from 400 to 750 nm are rapidly bleached along with greatly enhanced polaron absorption bands around 1000 nm and bipolaron absorption bands around 1400 nm. These findings show that a very effective doping process occurs under positive bias for all polymers. Importantly, when a negative bias of −0.4 V is applied, the absorption spectra of Pg2T-T and Pg2T-S significantly recover while the absorption intensity of Pg2T-SVS decreases even with negative bias. Because Pg2T-SVS has excellent electrochemical properties, as previously stated, we suspect that this decrease is originated from the change of film morphology caused by ion/water swelling, which would have a negative impact on the long-term operational stability of OECTs (vide infra).

Planar OECTs based on the three polymers were fabricated using the procedures described in the literature.[28] The polymers were spin-coated on substrates containing parylene packaged and patterned electrodes. The active layer was patterned using the peel-off approach, yielding an OECT width and length of 200 μm and 10 μm, respectively. The OECTs were then characterized in a 0.1 M NaCl aqueous electrolyte solution. The OECT output, transfer and transconductance curves are shown in Fig. 4a–f, and corresponding OECT parameters are summarized in Table 2. All polymers worked in the p-type accumulation mode, with high on/off ratios ranging from 10^4 to 10^5 magnitudes. The maximum transconductance ($g_{m,max}$) value of up to 12.29 mS, 14.45 mS, and 10.33 mS is reached for OECTs based on Pg2T-T, Pg2T-S, and Pg2T-SVS, respectively. According to the equation $g_m = \frac{Wd}{L}\mu C^*(V_{Th} - V_{GS})$, μC^* was calculated and summarized in Table 2 as the figure of merit for material performance comparison. The Pg2T-T based OECT shows a μC^* value of 288.9 F cm^{-1} V^{-1} s^{-1}, which is consistent with literature reports.[25] In comparison, Pg2T-S exhibits significantly higher OECT performance with a μC^* value of up to 332.7 F cm^{-1} V^{-1} s^{-1}, whereas Pg2T-SVS illustrates a slightly lower μC^* value of 285 F cm^{-1} V^{-1} s^{-1}. It should be noticed that the OECT performance of Pg2T-S differs from that in the current literature,[25] which could be attributed to differences in polymer molecular weights and film microstructures (vide infra). In addition, OECTs based on Pg2T-S and Pg2T-SVS have lower threshold voltages of −0.094 V and −0.148 V, respectively, compared to −0.161 V for Pg2T-T based OECTs (Fig. S5, ESI†). A low threshold voltage (less than −0.2 V) is beneficial for reducing energy consumption.[29–31] Electrochemical impedance

Table 1 Optical and electrochemical properties of Pg2T-T, Pg2T-S and Pg2T-SVS

Polymer	M_w [kDa]	$\lambda_{max,sol.}$ [nm]	$\lambda_{max,fil.}$[a] [nm]	E_{HOMO}[b] [eV]	E_{LUMO}[c] [eV]	$E_g^{opt\,d}$ [eV]
Pg2T-T	19.5	565	607 (653)	−4.29	−2.38	1.91
Pg2T-S	13.3	590	635 (684)	−4.29	−2.45	1.84
Pg2T-SVS	21.5	592	650 (704)	−4.43	−2.68	1.75

[a] The data in brackets represent shoulder peak. [b] E_{HOMO} calculated from the onset of oxidation peak (E_{ox}) using the equation $-E_{HOMO} = (E_{ox} - E_{Fc/Fc^+} + 4.8)$ eV. [c] According to the equation $E_{LUMO} = E_{HOMO} + E_g^{opt}$. [d] Calculated from the optical absorption on the set of polymer films using the equation $E_g^{opt} = 1240/\lambda_{onset}$.

7938 | J. Mater. Chem. C, 2024, **12**, 7935–7942

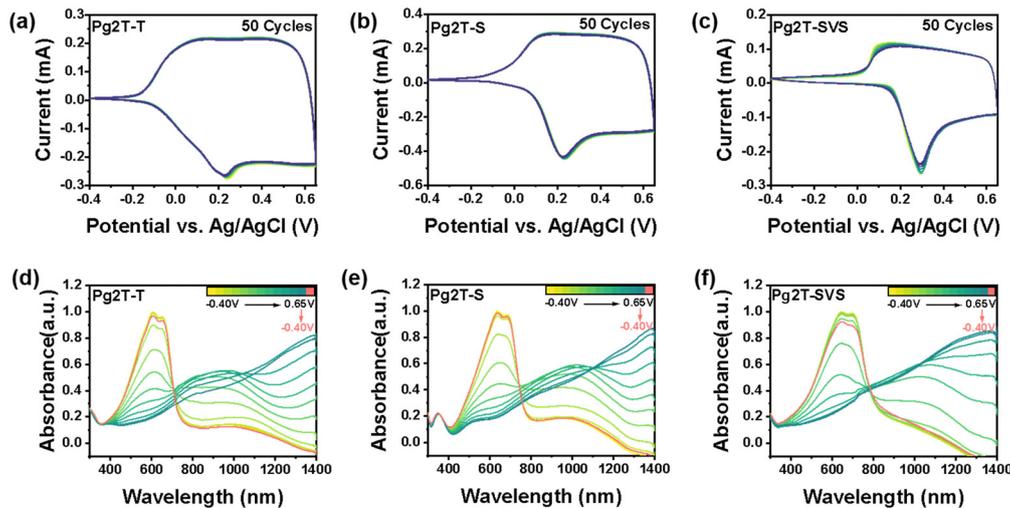This journal is © The Royal Society of Chemistry 2024

Fig. 3 CV scans of Pg2T-T (a), Pg2T-T (b), and Pg2T-SVS (c) thin films in 0.1 M NaCl aqueous solution after repeating for 50 cycles. UV-Vis-NIR spectroelectrochemical measurements of Pg2T-T (d), Pg2T-T (e), and Pg2T-SVS (f).
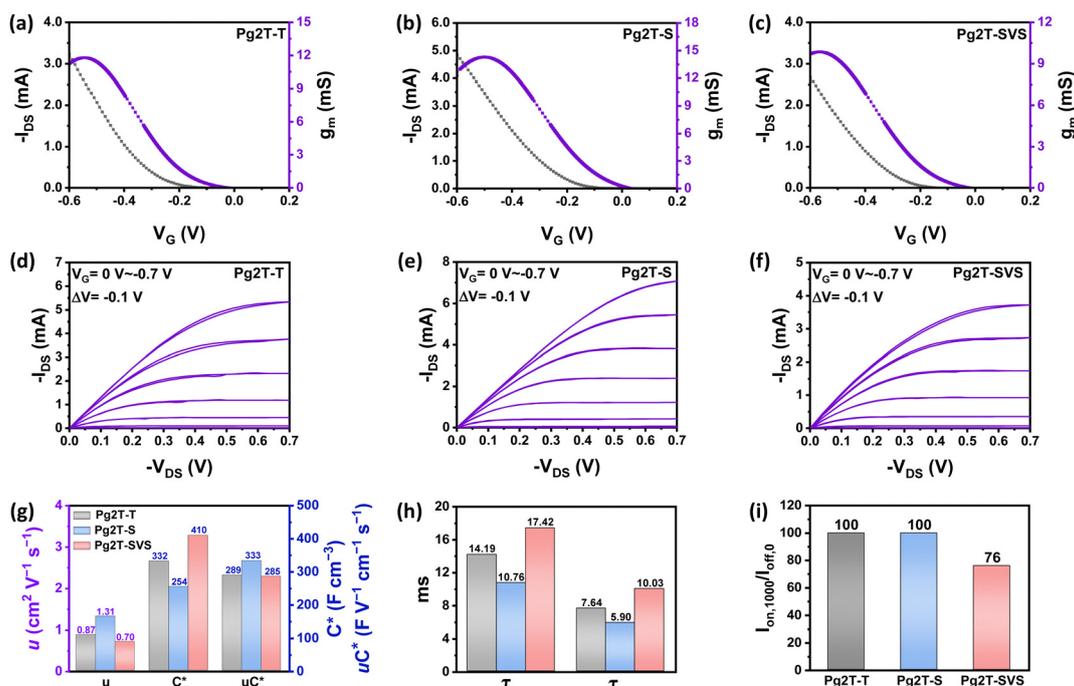

Fig. 4 The typical output, transfer and transconductance curves of (a) and (d) Pg2T-T, (b) and (e) Pg2T-S, and (c) and (f) Pg2T-SVS based OECTs. (g) Calculated μC^*, μ, and C^*, (h) τ_{on}/τ_{off} response time, and (i) retained ON current after 1000 cycles of Pg2T-T, Pg2T-S, and Pg2T-SVS based OECTs.

spectroscopy (EIS) was utilized to investigate the volumetric capacitance (C^*) of channel materials, as shown in Fig. S6 (ESI†) and Fig. 4g. The C^*s are extracted and summarized in Table S1 (ESI†) and Table 2. Pg2T-SVS delivers the highest C^* value of 410 F cm^{-3}, compared to 332 F cm^{-3} for Pg2T-T and 254 F cm^{-3} for Pg2T-S. Based on the μC^* and C^* values, the mobilities (μ) are calculated to be 0.87, 1.31, and 0.70 cm^2 V^{-1} s^{-1} for Pg2T-T, Pg2T-S, and Pg2T-SVS, respectively. To summarize the effect of selenium introduction on OECT performance, Pg2T-S exhibits

significantly improved μC^* with remarkably increased μ but slightly decreased C^*, while Pg2T-SVS showed comparable μC^* with significantly increased C^* but slightly decreased μ, when compared to selenium-free polymer Pg2T-T. The trade-off between μ and C^* may be altered by the combined effect of ion/water uptake and molecular packing, as previously observed.[32–36]

To evaluate the effect of selenium introduction on the OECT response speed, transient characteristics of OECT devices based on three polymers were carried out (Fig. S7, ESI† and

This journal is © The Royal Society of Chemistry 2024

J. Mater. Chem. C, 2024, **12**, 7935–7942 | **7939**

Paper

Journal of Materials Chemistry C

Table 2 Summary of the OECT performance parameters of Pg2T-T, Pg2T-S and Pg2T-SVS based OECTs

Polymer	d [nm]	$g_m{}^a$ [mS]	$V_{th}{}^b$ [V]	μC^{*c} [F V^{-1} cm^{-1} s^{-1}]	μ^d [cm^2 V^{-1} s^{-1}]	C^* [F cm^{-3}]	τ_{on} [ms]	τ_{off} [ms]	I_{on}/I_{off}
g2T-T	52	12.29	−0.161	288.9	0.87	332	14.19	7.64	10^4
g2T-S	46	14.45	−0.094	332.7	1.31	254	10.76	5.90	10^4
g2T-SVS	41	10.33	−0.148	285.0	0.70	410	17.42	10.03	10^5

All the OECT devices were operated in a 0.1 M NaCl aqueous solution. [a] Devices with the same channel dimensions were tested and counted for each polymer ($W/L = 200/10$ μm), $V_d = -0.5$ V. [b] The threshold voltage was determined by extrapolating the corresponding $I_d{}^{1/2}$ vs. V_g plots. [c] Materials' figure of merit μC^* was calculated from the measured transconductance. [d] Charge carrier mobility m was calculated from the μC^* and the measured volumetric capacitance C^*.

Fig. 4h). The response time (τ_{on} and τ_{off}) for each device was estimated *via* an exponential fitting of I_D and summarized in Table 2. Pg2T-S shows quickest response time, with a τ_{on}/τ_{off} value of 10.76 ms/5.9 ms, compared to 14.19 ms/7.64 ms for Pg2T-T and 17.42 ms/10.03 ms for Pg2T-SVS. The response time in the order of Pg2T-S < Pg2T-T < Pg2T-SVS is well in agreement with μC^* and μ in the sequence of Pg2T-S > Pg2T-T > Pg2T-SVS, since sufficiently high charge carrier mobility and fewer ions for doping/dedoping are extremely desirable for OECT with a fast response.[15,37,38] In addition to the transient characteristics, long-term stability throughout operation is a critical need for OECT-based applications. Therefore, device operational stability was investigated by monitoring the drain current during repeated gate pulsing for 1000 continuous ON–OFF cycles (Fig. S8, ESI† and Fig. 4i). Both Pg2T-T and Pg2T-S demonstrate outstanding operational stability, with 100% ON current retained after 1000 cycles. While Pg2T-SVS shows substantially weaker operational stability, keeping just 76% of the ON current, this could originate from larger C^*, which means more ion penetration and extraction as well as microstructure change.

To determine why Pg2T-SVS has a higher C^* value than others, the interaction between Cl$^-$ ions and cationic oligomer complexes was estimated using the Vienna *Ab initio* Simulation Package (VASP) based on the framework of the DFT.[39–41] The exchange–correlation energy was described by the generalized gradient approximation (GGA) using the Perdew–Burke–Ernzerhof (PBE) functional.[42] The plane-wave basis with a kinetic energy cutoff of 500 eV was employed. A vacuum of 25 Å was set along the a, b, and c axis to avoid the interaction between

the organic molecules. We calculated the binding energy E_b, defined as $E_b = (E_{tot} - E_{oc} - E_{Cl})$. Here, E_{tot}, E_{oc} and E_{Cl} are total energies of the Cl ion and cationic oligomer complexes, the oligomer complexes, and an isolated Cl ion. The binding energy rises from −0.645 eV for Pg2T-T to −0.999 eV for Pg2T-S and −1.237 eV for Pg2T-SVS, indicating that the interaction is gradually increasing. Fig. 5 shows the optimized structure diagram, the distance between oligomer and Cl$^-$ ion falls from 3.1 Å for Pg2T-T to 2.8 Å for Pg2T-S and 2.6 Å for Pg2T-SVS. It is consistent with the law of binding energy, as the bond length decreases, the interaction gradually increases. The results indicate that Pg2T-SVS is more favorable to interact with the Cl$^-$ ion, resulting in a higher C^* value. This is consistent with Pg2T-SVS's higher polarizability and dipole moment. Although Pg2T-S has larger binding energy and dipole moment than Pg2T-T, the C^* value decreases slightly, which is likely due to higher crystallinity that prevents ion penetration (*vide infra*).

As mentioned above, the crystallinity and packing orientation are critical factors in both charge transfer and ion/water uptake. Therefore, the film morphology was studied *via* atomic force microscopy (AFM) and grazing incidence wide angle X-ray scattering (GIWAXS),[43] as shown in Fig. 6 and Fig. S9 (ESI†). AFM analysis reveals that all films have substantially flat surface morphology. And as the selenium content increases, the root-mean-square (RMS) roughness values rise to 0.89 nm for Pg2T-S and 2.55 nm for Pg2T-SVS, compared to 0.78 nm for Pg2T-T. The results indicate the stronger aggregation behavior of Pg2T-S and Pg2T-SVS, which originates from increased intermolecular interaction of selenium-containing polymers. GIWAXS reveals varying structural orders in three polymers (Fig. 6, Fig. S10 and Table S2, ESI†). Pg2T-T exhibits face-on dominated orientation, with a lamellar diffraction peak (100) at $q = 0.33$ Å^{-1} (d-spacing of 1.90 nm) and a π–π stacking peak (010) at $q = 1.73$ Å^{-1} (d-spacing of 3.63 Å) oriented along the q_{xy} and q_z directions, respectively, while Pg2T-S exhibits significantly improved crystallinity, with lamellar diffraction peaks up to (300). More importantly, Pg2T-S exhibits mixed face-on and edge-on crystallite orientations, with lamellar peaks (100) (at $q = 3.1$ Å^{-1}, d-spacing = 2.03 nm) and a π–π stacking peak (at $q = 1.82$ Å^{-1}, d-spacing = 3.45 Å) in both q_{xy} and q_z directions. The higher crystallinity with mixed crystallite orientations and tight π–π stacking of Pg2T-S promote charge transport and limit ion penetration, resulting in higher μ but lower C^* compared to Pg2T-T. It should be noticed that the microstructure of Pg2T-S differs from that in the recent literature,[25] but is very similar to that reported by Huang *et al.*[44] which could be due to
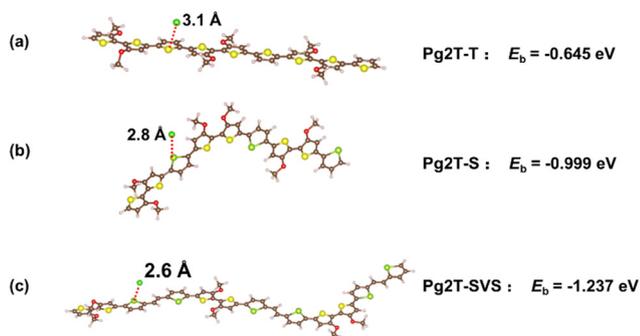

Fig. 5 Optimized geometries and binding energy of Cl ion and cationic oligomer complexes of (a) Pg2T-T⋯Cl$^-$, (b) Pg2T-S⋯Cl$^-$, and (c) Pg2T-SVS⋯Cl$^-$.
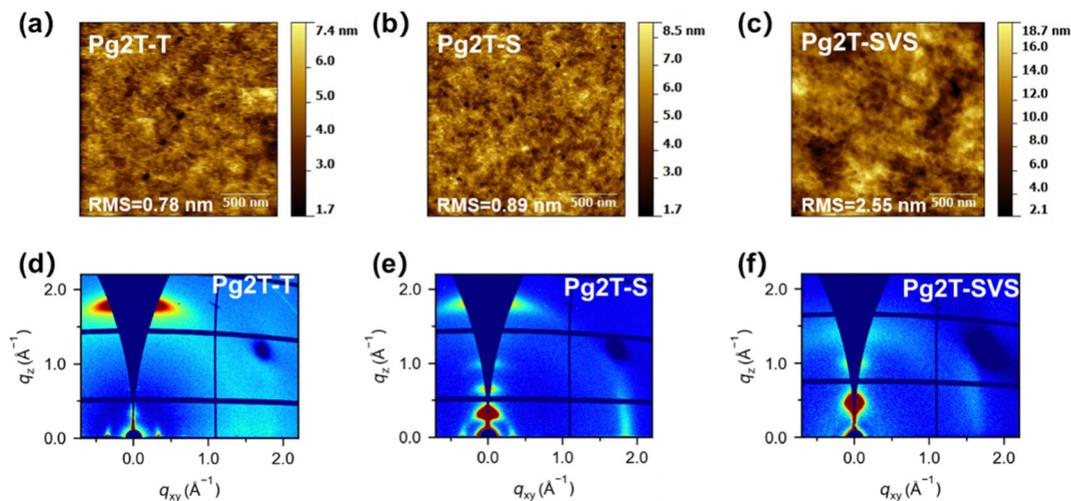
Fig. 6 AFM height images of (a) Pg2T-T, (b) Pg2T-S, and (c) Pg2T-SVS films. 2D-GIWAXS images of (d) Pg2T-T, (e) Pg2T-S, and (f) Pg2T-SVS films.

differences in molecular weight,[26] resulting in differing OECT performance. The GIWAXS pattern of Pg2T-SVS is extremely similar to that of p(g3T2-Te), which has well-oriented 3D crystallites as evidenced by strong and perfectly round (100) diffraction spots and mixed index scattering peaks.[25,45,46] Theoretically, such high crystallinity will facilitate charge transfer, but the OECT mobility is relatively lower than that of both Pg2T-T and Pg2T-S, which might be attributed to larger C^* (more bulk ions) that is damaging to the charge transport pathway.

Conclusions

In conclusion, we have systematically explored the influences of selenium incorporation on the optical, electrical, and electrochemical properties, as well as the OECT performance of polythiophene based OMIECs. We found that as the selenophene loading increases, the polymer dipole moment and the chloride ion (Cl^-)–polymer cation (P^+) binding energies increase from 1.12 Debye/-0.645 eV to 1.15 Debye/-0.999, and 1.99 Debye/-1.237 eV, for Pg2T-T, Pg2T-S, and Pg2T-SVS, respectively, due to the increased polarizability of the selenium atom. Both the above are beneficial for ion doping and volumetric capacitance, but harmful for charge transport. It is also observed that the crystalline orientation changed from face-on dominant for Pg2T-T to mixed for Pg2T-S and 3D for Pg2T-SVS, with the latter two being realized for a better charge transport pathway. For the Pg2T-S film, crystallinity and orientation play a superior role, leading to increased μ of 1.31 $cm^2 V^{-1} s^{-1}$ but decreased C^* of 254 F cm^{-3}. As a consequence, Pg2T-S demonstrates an increased μC^* of 332.7 F $cm^{-1} V^{-1} s^{-1}$ when compared to Pg2T-T (288.9 F $cm^{-1} V^{-1} s^{-1}$). However, Pg2T-SVS shows a slightly decreased μC^* of 285 F $cm^{-1} V^{-1} s^{-1}$, although having a larger volumetric capacitance of 410 F $cm^{-1} V^{-1} s^{-1}$. This high C^* could disrupt charge transfer, resulting in a lower μ of 0.695 $cm^2 V^{-1} s^{-1}$. We also observed that polymers with larger μ have faster turn-on and turn-off response times. We believe this systematic study will provide useful guidance for the development of selenium based OMIEC materials and high performance OECTs.

Conflicts of interest

There are no conflicts to declare.

Acknowledgements

References

1 A. Nawaz, Q. Liu, W. L. Leong, K. E. Fairfull-Smith and P. Sonar, *Adv. Mater.*, 2021, **33**, e2101874.

2 H. Sun, M. Vagin, S. Wang, X. Crispin, R. Forchheimer, M. Berggren and S. Fabiano, *Adv. Mater.*, 2018, **30**, 1704916.

3 H. Liu, J. Song, Z. Zhao, S. Zhao, Z. Tian and F. Yan, *Adv. Sci.*, 2024, 2305347.

4 Y. Yao, W. Huang, J. Chen, X. Liu, L. Bai, W. Chen, Y. Cheng, J. Ping, T. J. Marks and A. Facchetti, *Adv. Mater.*, 2023, **35**, 2209906.

5 W. Huang, J. Chen, Y. Yao, D. Zheng, X. Ji, L.-W. Feng, D. Moore, N. R. Glavin, M. Xie, Y. Chen, R. M. Pankow, A. Surendran, Z. Wang, Y. Xia, L. Bai, J. Rivnay, J. Ping, X. Guo, Y. Cheng, T. J. Marks and A. Facchetti, *Nature*, 2023, **613**, 496.

This journal is © The Royal Society of Chemistry 2024

J. Mater. Chem. C, 2024, **12**, 7935–7942 | **7941**

6 J. Chen, W. Huang, D. Zheng, Z. Xie, X. Zhuang, D. Zhao, Y. Chen, N. Su, H. Chen, R. M. Pankow, Z. Gao, J. Yu, X. Guo, Y. Cheng, J. Strzalka, X. Yu, T. J. Marks and A. Facchetti, *Nat. Mater.*, 2022, **21**, 564.

7 Y. Wang and Y. Liu, *Trends Chem.*, 2023, **5**, 279.

8 N. A. Kukhta, A. Marks and C. K. Luscombe, *Chem. Rev.*, 2022, **122**, 4325.

9 B. D. Paulsen, K. Tybrandt, E. Stavrinidou and J. Rivnay, *Nat. Mater.*, 2020, **19**, 13.

10 E. Zeglio and O. Inganas, *Adv. Mater.*, 2018, **30**, e1800941.

11 S. T. Keene, T. P. A. van der Pol, D. Zakhidov, C. H. L. Weijtens, R. A. J. Janssen, A. Salleo and Y. van de Burgt, *Adv. Mater.*, 2020, **32**, e2000270.

12 N. Wang, L. Xie, H. Ling, V. Piradi, L. Li, X. Wang, X. Zhu and F. Yan, *J. Mater. Chem. C*, 2021, **9**, 4260.

13 R. K. Hallani, B. D. Paulsen, A. J. Petty, 2nd, R. Sheelamanthula, M. Moser, K. J. Thorley, W. Sohn, R. B. Rashid, A. Savva, S. Moro, J. P. Parker, O. Drury, M. Alsufyani, M. Neophytou, J. Kosco, S. Inal, G. Costantini, J. Rivnay and I. McCulloch, *J. Am. Chem. Soc.*, 2021, **143**, 11007.

14 Y. Wang, S. Wustoni, J. Surgailis, Y. Zhong, A. Koklu and S. Inal, *Nat. Rev. Mater.*, 2024, **9**, 249.

15 S. Inal, G. G. Malliaras and J. Rivnay, *Nat. Commun.*, 2017, **8**, 1767.

16 C. B. Nielsen, A. Giovannitti, D. T. Sbircea, E. Bandiello, M. R. Niazi, D. A. Hanifi, M. Sessolo, A. Amassian, G. G. Malliaras, J. Rivnay and I. McCulloch, *J. Am. Chem. Soc.*, 2016, **138**, 10252.

17 A. Giovannitti, D. T. Sbircea, S. Inal, C. B. Nielsen, E. Bandiello, D. A. Hanifi, M. Sessolo, G. G. Malliaras, I. McCulloch and J. Rivnay, *Proc. Natl. Acad. Sci. U. S. A.*, 2016, **113**, 12017.

18 M. Moser, T. C. Hidalgo, J. Surgailis, J. Gladisch, S. Ghosh, R. Sheelamanthula, Q. Thiburce, A. Giovannitti, A. Salleo, N. Gasparini, A. Wadsworth, I. Zozoulenko, M. Berggren, E. Stavrinidou, S. Inal and I. McCulloch, *Adv. Mater.*, 2020, **32**, e2002748.

19 M. Moser, L. R. Savagian, A. Savva, M. Matta, J. F. Ponder, T. C. Hidalgo, D. Ohayon, R. Hallani, M. Reisjalali, A. Troisi, A. Wadsworth, J. R. Reynolds, S. Inal and I. McCulloch, *Chem. Mater.*, 2020, **32**, 6618.

20 B. Fan, F. Lin, X. Wu, Z. Zhu and A. K. Jen, *Acc. Chem. Res.*, 2021, **54**, 3906.

21 J. Ding, Z. Liu, W. Zhao, W. Jin, L. Xiang, Z. Wang, Y. Zeng, Y. Zou, F. Zhang, Y. Yi, Y. Diao, C. R. McNeill, C. A. Di, D. Zhang and D. Zhu, *Angew. Chem., Int. Ed.*, 2019, **58**, 18994.

22 F. Qi, F. R. Lin and A. K. Y. Jen, *Sol. RRL*, 2022, **6**, 2200156.

23 S. Ye, V. Lotocki, H. Xu and D. S. Seferos, *Chem. Soc. Rev.*, 2022, **51**, 6442.

24 W. Wu, K. Feng, Y. Wang, J. Wang, E. Huang, Y. Li, S. Y. Jeong, H. Y. Woo, K. Yang and X. Guo, *Adv. Mater.*, 2024, **36**, e2310503.

25 B. D. Paulsen, D. Meli, M. Moser, A. Marks, J. F. Ponder, R. Wu, E. A. Schafer, J. Strzalka, Q. Zhang, I. McCulloch and J. Rivnay, *Chem. Mater.*, 2024, **36**, 1818.

26 Y. Dai, S. Dai, N. Li, Y. Li, M. Moser, J. Strzalka, A. Prominski, Y. Liu, Q. Zhang, S. Li, H. Hu, W. Liu, S. Chatterji, P. Cheng, B. Tian, I. McCulloch, J. Xu and S. Wang, *Adv. Mater.*, 2022, **34**, e2201178.

27 Y. Xiao, H. Yao, Y. Yang, C. E. Song, J. Wang, N. Yang, Z. Li, Y. Yu, D. H. Ryu, C. An, W. S. Shin and J. Hou, *Sol. RRL*, 2023, **7**, 2300095.

28 J. Yu, P. Chen, C. W. Koh, H. Wang, K. Yang, X. Zhou, B. Liu, Q. Liao, J. Chen, H. Sun, H. Y. Woo, S. Zhang and X. Guo, *Adv. Sci.*, 2019, **6**, 1801743.

29 S. T. M. Tan, G. Lee, I. Denti, G. LeCroy, K. Rozylowicz, A. Marks, S. Griggs, I. McCulloch, A. Giovannitti and A. Salleo, *Adv. Mater.*, 2022, **34**, e2202359.

30 S. E. Doris, A. Pierre and R. A. Street, *Adv. Mater.*, 2018, **30**, e1706757.

31 H. Tseng, A. Weissbach, J. Kucinski, A. Solgi, R. Nair, L. M. Bongartz, G. Ciccone, M. Cucchi, K. Leo and H. Kleemann, *Adv. Mater. Interfaces*, 2022, **10**, 2201914.

32 P. Li and T. Lei, *J. Polym. Sci.*, 2021, **60**, 377.

33 M. Zhu, P. Li, J.-L. Li and T. Lei, *Mol. Syst. Des. Eng.*, 2022, **7**, 6.

34 L. Q. Flagg, C. G. Bischak, J. W. Onorato, R. B. Rashid, C. K. Luscombe and D. S. Ginger, *J. Am. Chem. Soc.*, 2019, **141**, 4345.

35 A. A. Szumska, I. P. Maria, L. Q. Flagg, A. Savva, J. Surgailis, B. D. Paulsen, D. Moia, X. Chen, S. Griggs, J. T. Mefford, R. B. Rashid, A. Marks, S. Inal, D. S. Ginger, A. Giovannitti and J. Nelson, *J. Am. Chem. Soc.*, 2021, **143**, 14795.

36 A. Savva, R. Hallani, C. Cendra, J. Surgailis, T. C. Hidalgo, S. Wustoni, R. Sheelamanthula, X. Chen, M. Kirkus, A. Giovannitti, A. Salleo, I. McCulloch and S. Inal, *Adv. Funct. Mater.*, 2020, **30**, 1907657.

37 H. Jia, Z. Huang, P. Li, S. Zhang, Y. Wang, J.-Y. Wang, X. Gu and T. Lei, *J. Mater. Chem. C*, 2021, **9**, 4927.

38 J. Rivnay, P. Leleux, M. Ferro, M. Sessolo, A. Williamson, D. A. Koutsouras, D. Khodagholy, M. Ramuz, X. Strakosas, R. M. Owens, C. Benar, J. M. Badier, C. Bernard and G. G. Malliaras, *Sci. Adv.*, 2015, **1**, e1400251.

39 G. Kresse and D. Joubert, *Phys. Rev. B: Condens. Matter Mater. Phys.*, 1999, **59**, 1758.

40 G. Kresse and J. Furthmüller, *Phys. Rev. B: Condens. Matter Mater. Phys.*, 1996, **54**, 11169.

41 K. J. Caulfield, R. Cooper and J. F. Boas, *Phys. Rev. B: Condens. Matter Mater. Phys.*, 1993, **47**, 55.

42 J. P. Perdew, K. Burke and M. Ernzerhof, *Phys. Rev. Lett.*, 1996, **77**, 3865–3868.

43 H. Li, S. Wang, X. Liu, F. Wu, Q. Zhang, J. Yuan, W. Ma and Y. Han, *Chem. Res. Chin. Univ.*, 2021, **38**, 1041.

44 L. Huang, Z. Wang, J. Chen, B. Wang, Y. Chen, W. Huang, L. Chi, T. J. Marks and A. Facchetti, *Adv. Mater.*, 2021, **33**, 2007041.

45 Z. Peng, L. Ye and H. Ade, *Mater. Horiz.*, 2022, **9**, 577.

46 J. Rivnay, S. C. B. Mannsfeld, C. E. Miller, A. Salleo and M. F. Toney, *Chem. Rev.*, 2012, **112**, 5488.

7942 | *J. Mater. Chem. C*, 2024, **12**, 7935–7942

This journal is © The Royal Society of Chemistry 2024